Quantum Electronics **39** (6) 575 – 582 (2009)

PACS numbers: 42.81.Dp; 42.81.Qb; 78.67.Ch
DOI: 10.1070/QE2009v039n06ABEH013959

Transmission of evanescent modes through a subwavelength aperture of a cylindrical waveguide. 2. The influence of dielectric properties of a real metal

T.I. Kuznetsova, V.S. Lebedev

Abstract. **The transmission of an evanescent light wave through the subwavelength aperture of a dielectric cylindrical metal-coated waveguide is studied. The theoretical approach to the description of the field structure in such a nanowaveguide is developed, which takes into account the transformation of the initial wave reflected from the output aperture and proves applicable when dielectric properties of a real metal are taken into account. The complex reflection coefficient of a supercritical waveguide mode from the aperture, the complex light flow and the far-field transmission coefficient are calculated for an aluminium-coated waveguide at the light wavelength of $\lambda = 488$ nm. It is established that the reflection and transmission coefficients of the nanowaveguide strongly depend on the dielectric constant of its core and differ significantly for transverse-magnetic and transverse-electric modes. It is demonstrated that the characteristics of light fields under study differ essentially from those of a nanowaveguide with ideally conducting walls and the subwavelength aperture in a perfectly conducting screen.**

Keywords: *evanescent electromagnetic wave, cylindrical nanowaveguide, subwavelength aperture, real metal.*

1. Introduction

In this paper, we present the results of the theoretical study of the transmission of an evanescent electromagnetic wave through a subwavelength output aperture of a cylindrical waveguide, which were obtained with allowance for the real dielectric properties both in the waveguide core and its metal coating. In other words, unlike the model problem we considered in [1], which is based on the ideal metal approximation, we will focus our main attention on the effects related to the finite dielectric constant of metal walls in a waveguide. The aim of this paper is to elucidate the role in the transmission of diffraction phenomena associated with the presence of the nanowaveguide output aperture and a jump in the dielectric constant at the nanowaveguide core – free space interface as well as the phenomena resulting from the excitation of surface plasmons in the metal coating.

Recently, the effects related to the influence of surface plasmons on the transformation of optical radiation upon its transmission through single subwavelength apertures in thin metal films or through a periodic system of nanoholes have been considered theoretically in many papers. These studies have been stimulated by the experimental discovery of a number of extraordinary resonance phenomena upon transmission of light through single subwavelength apertures or a system of periodic nanoholes in metal films (see [2 – 5] and reference therein). Among the theoretical papers we should mention, in particular, papers [6 – 10] aimed at studying the influence of dielectric properties of a metal on the light transmission by single nanoholes in thin and thick films of noble metals (Ag, Au) and at producing narrow-band light beams upon the transmission of light through a subwavelength aperture in a screen with a periodic corrugated structure [11 – 13]. The process of resonance transmission of light through a periodic system of holes in a metal was theoretically considered in papers [14 – 18]. It is also necessary to mention papers [19 – 21], which pointed out a significant role of the plasmon propagation during the transmission of radiation along metallized tapered walls of near-field optical probes.

Nevertheless, in many practically important cases, the role of diffraction phenomena during the transmission of light through the subwavelength aperture of a supercritical waveguide and the phenomena resulting from the excitation of surface plasmons in the waveguide metal coating remains unclear. The efficiency of light transmission in these problems strongly depends on the aperture diameter and the dielectric constants of the waveguide metal coating, its core and environment. In this paper, the elucidation of this problem is of key interest for us. We do not claim to consider all possible situations but study in detail a specific example which is of practical importance: the transmission of an evanescent light wave through a dielectric cylindrical waveguide coated with a real metal, for which the real part of the dielectric constant ε_m significantly exceeds its imaginary part: $\mathrm{Re}(-\varepsilon_m) \gg \mathrm{Im}\,\varepsilon_m$.

We have formulated the general theoretical approach to this problem, which allows one to involve into consideration the dielectric constant of the metal walls under conditions of small dissipation losses resulting from the finite conductivity

T.I. Kuznetsova P.N. Lebedev Physics Institute, Russian Academy of Sciences, Leninsky prosp. 53, 119991 Moscow, Russia; e-mail: tkuzn@sci.lebedev.ru;
V.S. Lebedev P.N. Lebedev Physics Institute, Russian Academy of Sciences, Leninsky prosp. 53, 119991 Moscow, Russia; Moscow Institute of Physics and Technology (State University), Institutskii per. 9, 141700 Dolgoprudnyi, Moscow region, Russia; e-mail: vlebedev@sci.lebedev.ru

Received 12 August 2008
Kvantovaya Elektronika **39** (6) 575 – 582 (2009)
Translated by I.A. Ulitkin

of the metal. The proposed approach is based, to a great extent, on theoretical results obtained in our paper [1]. We have performed a comparative analysis of the effect of the waveguide output hole on the field properties for the ideal and real metals and have calculated the reflection coefficient from the subwavelength output aperture, which is the main characteristic determining the field properties. We have also calculated the far-field transmission coefficient of light taking into account specific dielectric constants of the walls.

Calculations have been performed for the fields in aluminium-coated waveguides (the scheme of the waveguide is shown in Fig. 1 of paper [1]) at the radiation wavelength $\lambda = 488$ nm in cylindrical coordinates ρ, φ, z. As in [1], ε is the dielectric constant of the waveguide core ($0 \leqslant \rho < a$, $z < 0$, where a is the core radius of the waveguide), ε_m is the dielectric constant of the metal walls ($a \leqslant \rho < \infty$, $z < 0$) and ε_0 is the dielectric constant of the medium outside the waveguide ($z > 0$). For Al at $\lambda = 488$ nm we have $\varepsilon_m = -34.5 + i8.5$. In calculations we take into account only the real part of ε_m. The example of the transverse-magnetic mode TM_{01} is chosen for the main consideration. However, to demonstrate the strong dependence of the results on the spatial structure and the type of the waveguide modes, we have also calculated the transmission coefficients for the transverse-electric mode TE_{01}.

2. Calculation scheme of the fields in an infinite waveguide

First of all, we present expressions for the fields in an infinite (not truncated) waveguide with the walls having the negative dielectric constant. For propagating waves, the field parameters were studied in [22, 23]. Unlike these papers, we focus our attention on a supercritical waveguide, i.e. the fields damping in the axial direction. In the region of the waveguide core ($0 \leqslant \rho < a$), the expressions for the fields have the same form as in paper [1], namely:

$$\tilde{E}_\rho = CJ_1(q\rho)\exp\left[-z\left(q^2 - \frac{\omega^2\varepsilon}{c^2}\right)^{1/2}\right], \tag{1}$$

$$\tilde{E}_z = q\left(q^2 - \frac{\omega^2\varepsilon}{c^2}\right)^{-1/2} CJ_0(q\rho)\times \exp\left[-z\left(q^2 - \frac{\omega^2\varepsilon}{c^2}\right)^{1/2}\right], \tag{2}$$

$$\tilde{H}_\varphi = -\frac{i\omega\varepsilon}{c}\left(q^2 - \frac{\omega^2\varepsilon}{c^2}\right)^{-1/2} CJ_1(q\rho) \times \exp\left[-z\left(q^2 - \frac{\omega^2\varepsilon}{c^2}\right)^{1/2}\right], \tag{3}$$

where $J_0(x)$ and $J_1(x)$ are the Bessel function of the first order and its derivative; C is a constant. However, unlike expressions (1)–(3) from paper [1], the transverse wave numbers $q \equiv q_n = \xi_n/a$ and the number ξ_n will be different.

In the region of metal walls (i.e. at $a < \rho < \infty$) the field components of the TM_{01} mode will be expressed via the modified Bessel functions K_0 and K_1 :

$$\tilde{E}_\rho = CAK_1\left(\chi\frac{\rho}{a}\right)\exp\left[-z\left(q^2 - \frac{\omega^2\varepsilon}{c^2}\right)^{1/2}\right], \tag{4}$$

$$\tilde{E}_z = -\chi\left[a\left(q^2 - \frac{\omega^2\varepsilon}{c^2}\right)^{-1/2}\right] CAK_0\left(\chi\frac{\rho}{a}\right) \times \exp\left[-z\left(q^2 - \frac{\omega^2\varepsilon}{c^2}\right)^{1/2}\right], \tag{5}$$

$$\tilde{H}_\varphi = -\frac{i\omega\varepsilon_m}{c}\left(q^2 - \frac{\omega^2\varepsilon}{c\,2}\right)^{-1/2} CAK_1\left(\chi\frac{\rho}{a}\right) \times \exp\left[-z\left(q^2 - \frac{\omega^2\varepsilon}{c^2}\right)^{1/2}\right]. \tag{6}$$

Here, the constant A should be determined from the boundary conditions at $\rho = a$ and the number χ, characterising the field damping in the transverse direction in the walls is related to the number ξ by the expression

$$\xi^2 - a^2\frac{\omega^2\varepsilon}{c^2} = -\chi^2 - a^2\frac{\omega^2\varepsilon_m}{c^2}. \tag{7}$$

Hereafter, $\xi \equiv \xi_1$, where ξ_1 are the eigenvalues of the TM_{01} mode. The continuity condition of the tangential component of the electric field and the normal component of the electric inductance at the metal–dielectric interface yields

$$J_0(\xi)\xi = -AK_0(\chi)\chi, \quad J_1(\xi)\varepsilon = AK_1(\xi)\varepsilon_m. \tag{8}$$

By excluding the constant A from (8), we find

$$\xi\frac{J_0(\xi)}{J_1(\xi)} = -\frac{\varepsilon}{\varepsilon_m}\chi\frac{K_0(\chi)}{K_1(\chi)}. \tag{9}$$

Note that the system of equations similar to (7), (9) was obtained in [23] for propagating waves. In the case of evanescent waves, similar to paper [23], system (7), (9) allows one to find numbers ξ and χ for each specified value of ω/c.

3. Fields in a free space

Let us present expressions for the eigenwaves in the free space, which have the same symmetry as the waves in the waveguide (TM waves, $\partial/\partial\varphi = 0$). The field components of these waves are written in the form

$$E_\rho = CJ_1(\varkappa\rho)\exp\left[-z\left(\varkappa^2 - \frac{\omega^2\varepsilon_0}{c^2}\right)^{1/2}\right], \tag{10}$$

$$E_z = \varkappa\left(\varkappa^2 - \frac{\omega^2\varepsilon_0}{c^2}\right)^{-1/2} CJ_0(\varkappa\rho) \times \exp\left[-z\left(\varkappa^2 - \frac{\omega^2\varepsilon_0}{c^2}\right)^{1/2}\right], \tag{11}$$

$$H_\varphi = -\frac{i\omega\varepsilon}{c}\left(\varkappa^2 - \frac{\omega^2\varepsilon_0}{c^2}\right)^{-1/2} CJ_1(\varkappa\rho) \times \exp\left[-z\left(\varkappa^2 - \frac{\omega^2\varepsilon_0}{c^2}\right)^{1/2}\right]. \tag{12}$$

Here, unlike the case of the waveguide, where the wave number took the discrete values, the wave number $\varkappa$ can

take any values in the range from 0 to ∞. In expressions (10)–(12) at small $\varkappa$ (at $\varkappa^2 < \omega^2\varepsilon_0/c^2$) the quantity $(\varkappa^2 - \omega^2\varepsilon_0/c^2)^{1/2}$ is replaced by $-\mathrm{i}(\omega^2\varepsilon_0/c^2 - \varkappa^2)^{1/2}$. These expressions are valid only for the waves, which decay or propagate in the positive direction of the z axis. The exchange of z by $-z$ yields one more set of intrinsic solutions for an infinite space, which, however, will be of no use below when passing to the semi-infinite space. Note that the presented expressions for the fields have an identical form at any values of the transverse coordinate ρ, unlike the case of the waveguide fields, where, at $\rho < a$ and $\rho > a$, the functional dependence was different.

4. Fields in a truncated waveguide

Studying a truncated waveguide with walls made of a real metal, we should, in the general case, use the whole set of eigenmodes of an infinite waveguide, whose parameters are presented in section 2. However, if as an initial wave we use the evanescent wave corresponding to the only mode of an infinite waveguide, we can employ the same method as in the case of an open waveguide with an ideal metal coating [1]. Instead of the linear combination of different reflected modes with unspecified coefficients α_n, we can restrict ourselves to only one reflected wave and take only it into account in the expression for the complete field, by introducing the reflection coefficient α_1. Expressions for field components (1)–(3) after this allowance for reflected waves will take the form

$$\tilde{E}_\rho = CJ_1(q\rho)\left\{\exp\left[-z\left(q^2 - \frac{\omega^2\varepsilon}{c^2}\right)^{1/2}\right] + \alpha_1 \exp\left[z\left(q^2 - \frac{\omega^2\varepsilon}{c^2}\right)^{1/2}\right]\right\}, \tag{13}$$

$$\tilde{E}_z = q\left(q^2 - \frac{\omega^2\varepsilon}{c^2}\right)^{-1/2} CJ_0(q\rho)\left\{\exp\left[-z\left(q^2 - \frac{\omega^2\varepsilon}{c^2}\right)^{1/2}\right] - \alpha_1 \exp\left[z\left(q^2 - \frac{\omega^2\varepsilon}{c^2}\right)^{1/2}\right]\right\}, \tag{14}$$

$$\tilde{H}_\varphi = -\frac{\mathrm{i}\omega\varepsilon}{c}\left(q^2 - \frac{\omega^2\varepsilon}{c^2}\right)^{-1/2} CJ_1(q\rho) \times\left\{\exp\left[-z\left(q^2 - \frac{\omega^2\varepsilon}{c^2}\right)^{1/2}\right] - \alpha_1 \exp\left[z\left(q^2 - \frac{\omega^2\varepsilon}{c^2}\right)^{1/2}\right]\right\}. \tag{15}$$

Exactly as in (1)–(3), we replace the multiplier in expressions (4)–(6), which correspond to the fields in metal:

$$\tilde{E}_\rho = CAK_1\left(\chi\frac{\rho}{a}\right)\left\{\exp\left[-z\left(q^2 - \frac{\omega^2\varepsilon}{c^2}\right)^{1/2}\right] + \alpha_1 \exp\left[z\left(q^2 - \frac{\omega^2\varepsilon}{c^2}\right)^{1/2}\right]\right\}, \tag{16}$$

$$\tilde{E}_z = -\chi\left[a\left(q^2 - \frac{\omega^2\varepsilon}{c^2}\right)^{1/2}\right]^{-1} CAK_0\left(\chi\frac{\rho}{a}\right) \times\left\{\exp\left[-z\left(q^2 - \frac{\omega^2\varepsilon}{c^2}\right)^{1/2}\right] - \alpha_1 \exp\left[z\left(q^2 - \frac{\omega^2\varepsilon}{c^2}\right)^{1/2}\right]\right\}, \tag{17}$$

$$\tilde{H}_\varphi = -\frac{\mathrm{i}\omega\varepsilon_\mathrm{m}}{c}\left(q^2 - \frac{\omega^2\varepsilon}{c^2}\right)^{-1/2} CAK_1\left(\chi\frac{\rho}{a}\right) \times\left\{\exp\left[-z\left(q^2 - \frac{\omega^2\varepsilon}{c^2}\right)^{1/2}\right] - \alpha_1 \exp\left[z\left(q^2 - \frac{\omega^2\varepsilon}{c^2}\right)^{1/2}\right]\right\}. \tag{18}$$

Expressions (16)–(18) represent the first approximation to exact formulae for the fields in a truncated waveguide, which is similar to the first approximation to the solution in the case of an ideal metal considered earlier in [1]. In this case, the approximation obviously yields a small error, if the modulus of the dielectric constant of the walls is significantly larger than unity. A detailed analysis of the dependence of the error on the dielectric constant requires a separate investigation.

5. Fields in an open half-space behind the waveguide

In this section, we will construct the solution in the region adjacent to the waveguide in the form of an integral over the set of wave numbers according to expressions (10)–(12). Expressions for the field components have the form

$$E_\rho = \int_0^\infty B(\varkappa)J_1(\varkappa\rho)\exp[-\gamma(\varkappa)z]\varkappa\mathrm{d}\varkappa, \tag{19}$$

$$E_z = \int_0^\infty \exp[-\gamma(\varkappa)z]\frac{\varkappa J_0(\varkappa\rho)B(\varkappa)\varkappa\mathrm{d}\varkappa}{\gamma(\varkappa)}, \tag{20}$$

$$H_\varphi = -\frac{\mathrm{i}\omega\varepsilon_0}{c}\int_0^\infty B(\varkappa)J_1(\varkappa\rho)\exp[-\gamma(\varkappa)z]\frac{\varkappa\mathrm{d}\varkappa}{\gamma(\varkappa)}, \tag{21}$$

where

$$\gamma(\varkappa) = \begin{cases} -\mathrm{i}\left(\dfrac{\omega^2\varepsilon_0}{c^2} - \varkappa^2\right)^{1/2} & \text{for } \dfrac{\omega^2\varepsilon_0}{c^2} > \varkappa^2, \\ \left(\varkappa^2 - \dfrac{\omega^2\varepsilon_0}{c^2}\right)^{1/2} & \text{for } \dfrac{\omega^2\varepsilon_0}{c^2} \leqslant \varkappa^2. \end{cases} \tag{22}$$

The expansion coefficient $B(\varkappa)$ is determined from the continuity condition of the component E_ρ at $z = 0$, i.e. from the equation

$$\tilde{E}_\rho(\rho, 0) = E_\rho(\rho, 0), \tag{23}$$

in full agreement with the way it was done in [1]. Because of a more complex (compared to the case of an ideal metal) field structure at $z < 0$, we obtain the expression for $B(\varkappa)$ of a more complicated form than that in paper [1]:

$$B(\varkappa) = (1 + \alpha_1)Ca^2\left\{\frac{1}{-(\varkappa a)^2 + \xi^2}[\varkappa aJ_0(\varkappa a)J_1(\xi) - \xi J_1(\varkappa a)J_0(\xi)] - \frac{1}{(\varkappa a)^2 + \chi^2}\frac{\varepsilon}{\varepsilon_\mathrm{m}}\frac{J_1(\xi)}{K_1(\chi)} \times[\varkappa aJ_0(\varkappa a)K_1(\chi) - \chi J_1(\varkappa a)K_0(\chi)]\right\}. \tag{24}$$

Recall that the numbers of ξ and χ entering into expression (24) are determined from system of equations (7), (9). The results of specific calculations of ξ and χ for the nano-

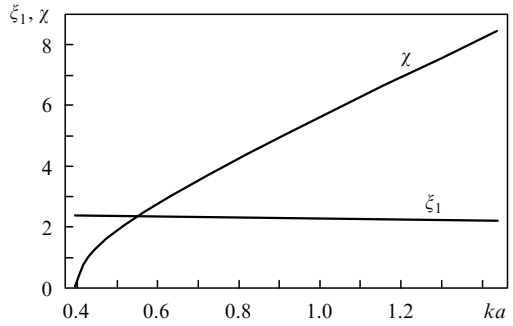

Figure 1. Dependences of the dimensionless parameter χ and eigenvalue $\xi \equiv \xi_1$ of the lowest transverse-magnetic mode TM_{01} on ka ($k = \omega\varepsilon_0^{1/2}/c$). Calculations are performed in the range of values $0.3967 < ka < 1.4364$ for which this waveguide mode exists and is evanescent.

waveguide with a glass core ($\varepsilon = 2.25$) and an aluminum coating are presented in Fig. 1 for 488-nm radiation, when $\mathrm{Re}\,\varepsilon_m = -34.5$. The dielectric constant of the environment ε_0 was taken equal to unity.

The choice of the function of type (24) as the expansion coefficient $B(\varkappa)$ *a fortiori* guarantees the continuity of the tangential component of the electric field E_{tang}. As for the conjugation of the magnetic field components H_{tang}, then, according to the results of paper [1], instead of the field equality we will require the equality of complex flows.

6. Complex flow inside the waveguide and in the external space

In paper [1] we introduced and used in calculations complex flows integrated in the output waveguide aperture ($\tilde{j}$ and j), and derived expressions for such flows, where we took into account the symmetry of the waveguide and the fields under study. Here, the definition of the flow is somewhat modified. We will consider renormalised complex flows $\tilde{S}$ and S differing from the previous ones ($\tilde{j}$ and j) by the constant multiplier $c/4$. The passage to the renormalised flows somewhat simplifies the final expressions for the far-field transmission efficiency of radiation and decreases the number of intermediate expressions required to calculate the fields of a truncated waveguide.

Let us introduce the complex flows $\tilde{S}$ and S with the help of expressions

$$\tilde{S} = \int_0^\infty [\tilde{\boldsymbol{E}}, \tilde{\boldsymbol{H}}^*]_z \rho \mathrm{d}\rho, \quad S = \int_0^\infty [\boldsymbol{E}, \boldsymbol{H}^*]_z \rho \mathrm{d}\rho. \tag{25}$$

By substituting expressions (13), (15), (16), (18) for the fields inside the waveguide into the expression for $\tilde{S}$, we have

$$\tilde{S} = \int_0^\infty \tilde{E}_\rho(\rho,0)\tilde{H}_\varphi^*(\rho,0)\rho \mathrm{d}\rho = \frac{\mathrm{i}\omega}{c}|C|^2(1+\alpha_1)(1-\alpha_1^*)a^3 \times \left[2\left(\xi^2 - a^2\frac{\omega^2\varepsilon}{c^2}\right)^{1/2}\right]^{-1}\left[\varepsilon I_a + \frac{\varepsilon^2}{\varepsilon_m}\frac{J_1^2(\xi)}{K_1^2(\chi)} I_\infty\right], \tag{26}$$

where the notations

$$I_a = J_1^2(\xi) - J_0(\xi)J_2(\xi), \quad I_\infty = -\left[K_1^2(\chi) - K_0(\chi)K_2(\chi)\right] \tag{27}$$

are used and it is taken into account that according to (8), expression for the constant A has the form

$$A = \frac{\varepsilon}{\varepsilon_m}\frac{J_1(\xi)}{K_1(\chi)}. \tag{28}$$

We will express now the complex flow through the characteristics of the external fields. By substituting relations (19), (21), (24) into the second expression in (25) for the flow, and by changing the integration order and integrating initially over $\rho \mathrm{d}\rho$ and then over $\mathrm{d}\varkappa$, we obtain

$$S = \int_0^\infty E_\rho(\rho,0)H_\varphi^*(\rho,0)\rho \mathrm{d}\rho = a^3\frac{\mathrm{i}\omega\varepsilon_0}{c}|C|^2|1+\alpha_1|^2 I^*. \tag{29}$$

Expression (29) includes integration over $\mathrm{d}\varkappa$ which will be denoted by I^*. The imaginary and real parts of the integral $I = \mathrm{Re}\,I + \mathrm{i}\mathrm{Im}\,I$ are expressed by

$$\mathrm{Re}\,I = \int_{a\omega\varepsilon_0^{1/2}/c}^\infty \left(x^2 - a^2\frac{\omega^2\varepsilon_0}{c^2}\right)^{-1/2}\psi(x)x\mathrm{d}x,$$
$$\mathrm{Im}\,I = \int_0^{a\omega\varepsilon_0^{1/2}/c} \left(a^2\frac{\omega^2\varepsilon_0}{c^2} - x^2\right)^{-1/2}\psi(x)x\mathrm{d}x, \tag{30}$$

and the function $\psi(x)$ in integrand (30) has the form

$$\psi(x) = \left\{\frac{1}{-x^2+\xi^2}[xJ_0(x)J_1(\xi) - \xi J_1(x)J_0(\xi)] + \frac{1}{x^2+\chi^2}\frac{\varepsilon}{\varepsilon_m}\frac{J_1(\xi)}{K_1(\chi)}[xJ_0(x)K_1(\chi) - \chi J_1(x)K_0(\chi)]\right\}^2. \tag{31}$$

Equalities (26) and (29) allow one to represent the continuity expression of the complex flow $\tilde{S} = S$ in the form

$$(1-\alpha_1^*)M = (1+\alpha_1^*)I^*. \tag{32}$$

The quantity M in (32) is given by the expression

$$M = \left[2\varepsilon_0\left(\xi^2 - a^2\frac{\omega^2\varepsilon}{c^2}\right)^{1/2}\right]^{-1}\left(\varepsilon I_a + |A|^2\varepsilon_m I_\infty\right). \tag{33}$$

Expression (32) together with expressions (27), (28), (30), (31) and (33) makes it possible to determine the main characteristic – the reflection coefficient α_1.

Note once again that the condition

$$\tilde{S} = S \tag{34}$$

lays the basis of our approach. In other words, we require the equality of complex flows inside and outside the waveguide instead of the equality of magnetic fields H_φ and $\tilde{H}_\varphi$ at each point of the output aperture. Thus, we construct the solution meeting the weakest condition, than is required by the rigorous approach, which facilitates the procedure of the solution construction.

Recall that in the case of rather simple geometry (when the ratio E/H is independent of the transverse coordinate), the continuity condition E/H together with the continuity condition of the tangential component of the electric field, i.e. when E_ρ and $\tilde{E}_\rho$ coincide, gives a more complete formulation of boundary conditions for the fields at the interface of two media. In this paper instead of ratio E/H, we introduce the ratio of the quantity

$$W_\rho = \int_0^\infty E_\rho^*(\rho,0)E_\rho(\rho,0)\rho \mathrm{d}\rho \tag{35}$$

to the quantity S^*:

$$\frac{W_\rho}{S^*} = \int_0^\infty E_\rho^*(\rho,0)E_\rho(\rho,0)\rho \mathrm{d}\rho \Big/ \int_0^\infty E_\rho^*(\rho,0)H_\varphi(\rho,0)\rho \mathrm{d}\rho, \tag{36}$$

and try to achieve coincidence of the values of this ratio at $z = -0$ and $z = +0$. The introduced characteristic can be considered as the aperture impedance in the bulk metal bordering the open space. The use of this characteristic makes it possible to obtain solutions in the case of a more complex geometry when the ratio E/H depends on the transverse coordinates.

The quantity W_ρ is proportional to the integrated energy density, which is related to the tangential component of the electric field,

$$\mathscr{W}_\rho = \frac{\varepsilon_0}{16\pi}\int_0^{2\pi} \mathrm{d}\varphi \int_0^\infty E_\rho^*(\rho,0)E_\rho(\rho,0)\rho \mathrm{d}\rho = \frac{\varepsilon_0}{8}\, W_\rho. \tag{37}$$

By using expressions (13) and (16) for $\tilde{E}_\rho$, we obtain the following result for W_ρ – renormalised energy density, integrated in aperture:

$$W_\rho = |1+\alpha_1|^2 \frac{a^2}{2} |C|^2 (I_a + |A|^2 I_\infty). \tag{38}$$

The ratios of the complex flow in the waveguide and in the free space to the integrated energy density have the form

$$\frac{\tilde{S}}{W_\rho} = \frac{\mathrm{i}a\omega}{c}\frac{1-\alpha_1^*}{1+\alpha_1^*}\left(\xi^2 - a^2\frac{\omega^2\varepsilon}{c^2}\right)^{-1/2} \frac{\varepsilon I_a + |A|^2\varepsilon_\mathrm{m} I_\infty}{I_a + |A|^2 I_\infty}, \tag{39}$$

$$\frac{S}{W_\rho} = a\frac{2\mathrm{i}\omega}{c}\frac{\varepsilon_0 I^*}{I_a + |A|^2 I_\infty}. \tag{40}$$

Expressions (29), (30) and (38) obtained in this section give more complete information on the electromagnetic energy density directly at the waveguide output, i.e. in the near-field zone, and on the energy flux in the far-field zone. To compare the case of the real metal with that of the ideal metal we present limiting expressions, to which expressions (29), (30) and (38) are transformed at $|\varepsilon_\mathrm{m}| \to \infty$.

7. Passage to the limit of an ideal metal

Note that expressions from paper [1] corresponding to the ideal metal are a particular case of expressions presented in section 6. In fact, if the dielectric constant ε_m in the region $\rho > a$, $z < 0$ indefinitely increases in modulus, the electric field in the waveguide walls vanishes and the eigenvalues ξ becomes equal to the root of the equation $J_0(x) = 0$. In this case, the contribution to the flow calculated at $z = -0$ will be made only by the waveguide core and expression (26) will assume the form

$$\tilde{S} = \frac{\mathrm{i}\omega}{c}|C|^2(1+\alpha_1)(1-\alpha_1^*)a^3\left[2\left(\xi^2 - a^2\frac{\omega^2\varepsilon}{c^2}\right)^{1/2}\right]^{-1}\varepsilon I_a, \tag{41}$$

the quantity I_a being given by the expression

$$I_a = J_1^2(\xi). \tag{42}$$

The integral of the square of the tangential component of the electric field will be expressed by a simple equation

$$W_\rho = |1+\alpha_1|^2\frac{a^2}{2}|C|^2 I_a. \tag{43}$$

The expressions related to the free space are simplified as well. In calculating the field in the region $z > 0$, the expression for the coefficient $B(\varkappa)$ will contain only the contribution from the field in the waveguide core:

$$B(\varkappa) = (1+\alpha_1)Ca^2\frac{1}{\xi^2 - (\varkappa a)^2}\varkappa a J_0(\varkappa a)J_1(\xi), \tag{44}$$

which, taking into account the only reflected wave, exactly corresponds to expressions (12) and (14) from paper [1]. In this case, in the integral I [see (30)], the integrand is simplified and the expression for it will assume the form

$$\psi(x) = \left[\frac{xJ_0(x)}{\xi^2 - x^2}\right]^2 J_1^2(\xi), \tag{45}$$

and the integral I will be expressed via I_{11} obtained in [1], i.e. we deal with the equality

$$I = J_1^2(\xi) I_{11}. \tag{46}$$

In this case, the expression for the flow S takes the form

$$S = a^3\frac{\mathrm{i}\omega\varepsilon_0}{c}|C|^2|1+\alpha_1|^2 J_1^2(\xi) I_{11}^*, \tag{47}$$

corresponding to the results of paper [1].

Now, using equalities (41), (42), (47) and (43) we obtain the ratio between W_ρ and complex flows inside ($\tilde{S}$) and outside (S) the waveguide:

$$\frac{\tilde{S}^*}{W_\rho} = a\frac{\mathrm{i}\omega}{c}\varepsilon\left(q_1^2 - \frac{\omega^2\varepsilon}{c^2}\right)^{-1/2}\left(\frac{1-\alpha_1}{1+\alpha_1}\right). \tag{48}$$

$$\frac{S^*}{W_\rho} = -a\frac{2\mathrm{i}\omega\varepsilon_0}{c} I_{11}. \tag{49}$$

Note that expression (48) in the explicit form relates the flow with the reflection coefficient. Expression (49) equivalent to (48) (due to the flow continuity) makes it possible to express the real and imaginary parts of the ratio S/W_ρ via the integral I_{11}, which is a quantitative parameter of the scheme considered taking into account its parameters [see (30)]. These expressions have the form

$$\frac{\mathrm{Re}\, S}{W_\rho} = a\frac{2\omega\varepsilon_0}{c}\,\mathrm{Im}\, I_{11}, \tag{50}$$

$$\frac{\mathrm{Im}\, S}{W_\rho} = a\frac{2\omega\varepsilon_0}{c}\,\mathrm{Re}\, I_{11}. \tag{51}$$

The first of these ratios in the region of small values ka ($k = \omega\varepsilon_0^{1/2}/c$ is the wave number) takes a simple form:

$$\frac{\mathrm{Re}\, S}{W_\rho} = \frac{4\varepsilon_0^{1/2}}{3\xi_1^4}(ka)^4 = 0.03987\varepsilon_0^{1/2}(ka)^4. \tag{52}$$

8. Results of calculations of the reflection coefficient and the complex flow for a nanowaveguide with aluminium walls

In section 6 we derived expression (32), which can help to determine the reflection coefficient . The final expression for α_1 has the form

$$\alpha_1 = \frac{1 - I/M}{1 + I/M}. \tag{53}$$

This expression together with (30), (31) and (33) generalises the results of our previous paper {see expressions (20), (21) and (26) in [1]} to the case of waveguide walls made of a real metal.

Based on the above expressions, we calculated the reflection coefficient from the aperture of the nanowaveguide with a glass core ($\varepsilon = 2.25$) and an aluminium coating ($\mathrm{Re}\,\varepsilon_m = -34.5$) for 488-nm radiation. The dielectric constant of the environment ε_0 was assumed equal to unity. For this waveguide, the results of calculations of the real and imaginary parts of α_1 as a function of ka are presented in Fig. 2. The same figure presents the results obtained for the waveguide with the walls made of an ideal metal. The comparison of the curves shows that the dependence of the reflection coefficient on ka is qualitatively the same under the condition that an evanescent mode exists in an aluminium-coated waveguide. This condition has the form $ka > x_{\min}^{\mathrm{Al}}$ and $x_{\min}^{\mathrm{Al}} = 0.3967$ is the point at which χ determined by expressions (7), (9) vanishes, i.e. at a small radius of the core the walls do not hold the mode any more.

It follows from Fig. 2 that the curves in both cases are especially close in the interval $x_{\min}^{\mathrm{Al}} < ka \lesssim 1$. At $0 < ka < x_{\min}^{\mathrm{Al}}$, the mode under study disappears in the aluminium-coated waveguide, which means that in this region the model of an ideal metal is inapplicable. One can also see that with increasing ka, the differences for the waveguides with coatings made of an ideal and real metals increase. The differences turn the largest in the vicinity of points $x_{\max}^{\mathrm{Al}}$, where $x_{\max}^{\mathrm{Al}} = \xi_1^{\mathrm{Al}}\ (\varepsilon_0/\varepsilon)^{1/2} = 1.4364$ ($\xi_1^{\mathrm{Al}} = 2.1547$). Starting from point $ka > 1.4364$, the evanescent mode becomes propagating. Recall that in the case of an ideal metal (when $\xi_1^{\mathrm{id}} = 2.4048$) this occurs at $x_{\max}^{\mathrm{id}} = \xi_1^{\mathrm{id}}(\varepsilon_0/\varepsilon)^{1/2} = 1.6032$. On the whole, the calculation performed allow one to draw the conclusion that for a metal with a negative dielectric constant that is high with respect to the absolute value, the ideal metal model is applicable in a rather broad range of parameters.

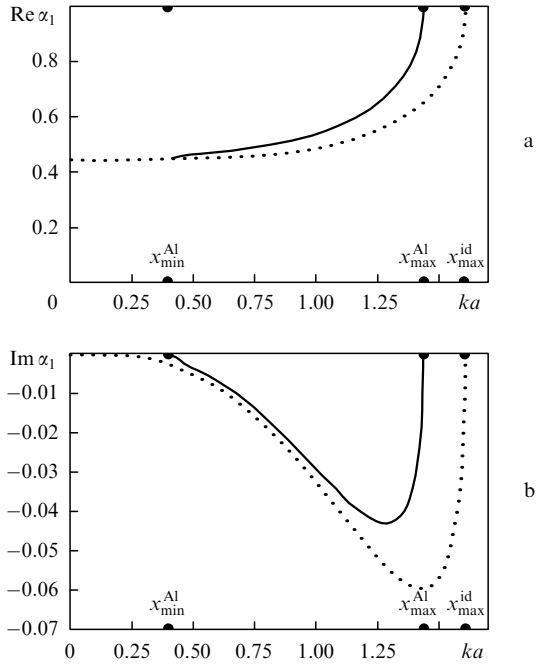

Figure 2. Real (a) and imaginary (b) parts of the amplitude reflection coefficient α_1 of the evanescent TM_{01} wave from the subwavelength waveguide aperture as a function of ka. Solid curves are the results of calculations for the aluminium-coated waveguide with the fused-silica core ($\varepsilon = 2.25$) at $\lambda = 488$ nm and $\varepsilon_0 = 1$; dashed curves – for the waveguide with ideally conducting walls.

The results of calculations of the real and imaginary parts of the ratio of the complex flow S (25) to the integrated energy density W_ρ of the transverse component of the electric field (35) are presented in Fig. 3 for the TM_{01} mode under study. The comparison of the results obtained for the waveguides with coatings made of real (aluminium) and ideal metals shows that they are in good agreement in the region $x_{\min}^{\mathrm{Al}} < ka < x_{\max}^{\mathrm{Al}}$, in which the evanescent mode in the aluminium-coated waveguide exists.

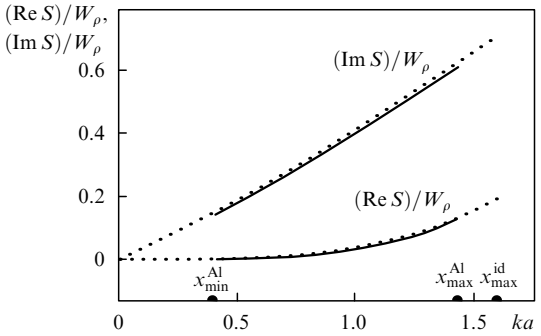

Figure 3. Ratio of the real and imaginary parts of the complex flow S (25) to the integrated energy density W_ρ of the transverse component of the electric field (35) as a function of ka. Solid curves are the results of calculations for the aluminium-coated waveguide with the fused-silica core ($\varepsilon = 2.25$) at $\lambda = 488$ nm and $\varepsilon_0 = 1$; dashed curves – for the waveguide with ideally conducting walls.

9. Energy flux and far-field transmission coefficient

The results obtained in section 6 for the complex flow allow one to calculate the far-field transmission coefficient of radiation and express it through the reflection coefficient of a decaying wave whose field is perturbed due to the presence of an output hole. The far-field transmission coefficient is the parameter, which is usually used to estimate the efficiency of the near-field probes. This coefficient characterising the electromagnetic wave was first introduced in papers [24, 25], which considered the transmission of a plane wave through a pin hole in an ideally conducting screen. It was defined as a ratio of the flux appearing behind the pin hole in the screen to the incident flux (which would take place in the absence of the perturbing action of the screen and aperture):

$$T = \frac{\mathrm{Re}\left(\iint E_{\mathrm{tang}} H_{\mathrm{tang}}^{*} \rho \mathrm{d}\rho \mathrm{d}\varphi\right)}{\iint E_{\mathrm{tang}}^{\mathrm{inc}} \left(E_{\mathrm{tang}}^{\mathrm{inc}}\right)^{*} \rho \mathrm{d}\rho \mathrm{d}\varphi}. \tag{54}$$

Here we transformed the expression for the transmission coefficient from papers [24, 25] by using the fact that in the plane wave the initial amplitudes of the fields $E_{\mathrm{tang}}^{\mathrm{inc}}$ and $H_{\mathrm{tang}}^{\mathrm{inc}}$ are equal. Then we rewrote this expression in the form suitable for the supercritical waveguide. Based on expres-

sion (54), we can express the transmission coefficient of a truncated waveguide via the quantities found in the previous sections. We derive the required expression taking into account that the resultant field at the waveguide output (in the approximation under study) differs from the initial unperturbed field by the multiplier $(1+\alpha_1)$. It is also necessary to take into account that the fields of the TM_{01} mode are independent of the angular coordinate φ. In this case, we obtain from Eqns (29), (38) and (54) the final expression for the T coefficient in the form

$$T = |1+\alpha_1|^2 \frac{\mathrm{Re}(\iint E_\rho H_\varphi^* \rho \mathrm{d}\rho \mathrm{d}\varphi)}{\iint E_\rho E_\rho^* \rho \mathrm{d}\rho \mathrm{d}\varphi} \equiv \frac{\mathrm{Re}\, S}{W_\rho} |1+\alpha_1|^2. \quad (55)$$

Based on expression (55) we calculated the far-field transmission coefficient T. The results obtained for the aluminium-coated waveguide and the waveguide with ideally conducting walls are shown in Fig. 4. One can see that the dependences T on ka are close to each other in the region of existence of the waveguide TM_{01} mode under study in the case of the real metal (i.e. at $0.3967 < ka < 1.4364$). However, the ideal metal model is inapplicable in the region of small wave numbers, $0 < ka < 0.3967$ (where the waveguide mode disappears) and in the region $1.4364 < ka < 1.6032$ due to the decrease in the values $x_{\max} \equiv (ka)_{\max}$ in the case of the real metal compared to the case of ideal metal; starting from this value, the evanescent mode is transformed into the propagating one ($x_{\max}^{\mathrm{Al}} = 1.4364$ and $x_{\max}^{\mathrm{id}} = 1.6032$). These differences manifest themselves in comparison of the values of the transmission coefficient T multiplied by $(ka)^{-4}$ for the case of the real and ideal metals (see inset in Fig. 4).

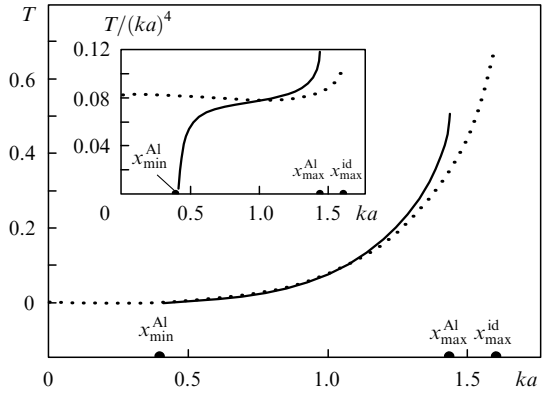

Figure 4. Far-field transmission coefficient T for the aluminium-coated waveguide (solid curve) and the waveguide with ideally conducting walls (dashed curve) as a function of ka. The inset shows the dependence of $T/(ka)^4$ on ka. Calculations have been performed for the TM_{01} mode in the waveguide with a fused silica core ($\varepsilon = 2.25$) at $\lambda = 488$ nm and $\varepsilon_0 = 1$.

Figure 5 presents the dependence of the coefficient T multiplied by $(ka)^{-4}$ on the quantity ka for the waveguide with an ideal metal coating. Calculations are performed for the TM_{01} mode by using expressions (55) and (50). One can see that the asymptotic behaviour of $T/(ka)^4$ at small ka agrees with dependence (52) obtained in section 7. To demonstrate the dependence of the transmission efficiency on the types of waveguide modes, Fig. 5 shows the results of calculations for the transverse-electric mode TE_{01} and the transmission of light through the subwavelength aperture in the screen, calculations being obtained within the framework of the theory [24, 25]. The TE_{01} mode was theoretically analysed with the help of the method similar to that reported in this paper as applied to the TM_{01} mode (the derived expression in this case will be presented elsewhere). One can see from Fig. 5 that the transmission coefficient strongly depends on the type of the initial mode: for the TM_{01} mode it is approximately eight times larger that for the TE_{01} mode. As for the comparison with the result of the classical theory [24, 25] (initial plane wave), the transmission coefficient exceeds its value by 6.02 and 48.93 times for TM_{01} and TE_{01} modes, respectively, in the region $ka \ll 1$.

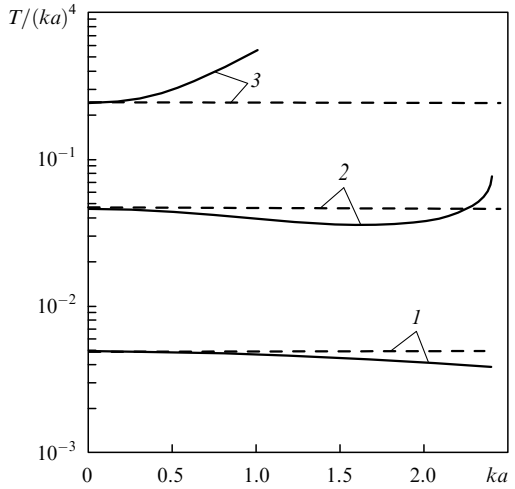

Figure 5. Far-field transmission coefficient T divided by $(ka)^4$ as a function of ka. Solid curves (*1*, *2*) are the results of calculations by the general expressions for the TE_{01} (*1*) and TM_{01} (*2*) modes; dashed curves (*1*, *2*) are the results of calculations with the help of asymptotic expressions ($ka \ll 1$) for the same modes. Solid curve (*3*) is the transmission of a linearly-polarised plane wave through a pin hole in an ideally conducting screen [25]; dashed curve (*3*) described the contribution of the first term in the expansion of the solution obtained in [25], which corresponds to the known result of paper [24].

Figure 6 demonstrates that the far-field transmission coefficient of light significantly depends on the dielectric constant ε of the waveguide core. According to the results obtained, the increase in ε leads to the increase in the transmission efficiency at one and the same ka. However, the range of ka values at which the waveguide mode is evanescent ($ka < x_{\max}$), decreases in accordance with the relation $x_{\max} = \xi(\varepsilon_0/\varepsilon)^{1/2}$.

10. Conclusions

(i) The ideal-metal-approximation approach [1] to the description of the transmission of an evanescent wave through a subwavelength aperture of a cylindrical waveguide is generalised to the case of the real metal, whose real part of the dielectric constant in modulus markedly exceeds its imaginary part [$\mathrm{Re}(-\varepsilon_{\mathrm{m}}) \gg \mathrm{Im}\varepsilon_{\mathrm{m}}$]. Explicit expressions have been obtained for the reflection coefficient of the supercritical waveguide mode from the aperture, the complex light flow at the waveguide output as well as for the energy flux and the far-field transmission coefficient of the nanowaveguide. Numerical calculations have been

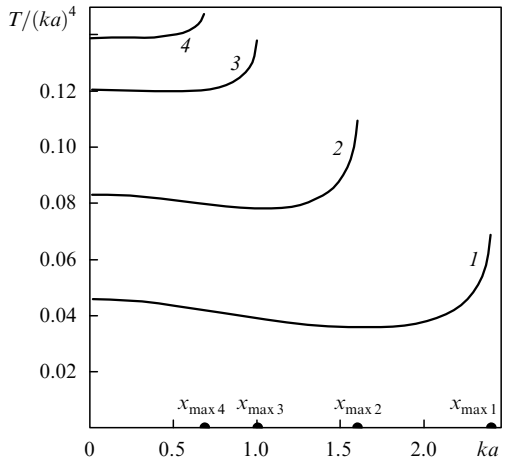

Figure 6. Far-field transmission coefficient T divided by $(ka)^4$ as a function of ka. Curves (*1*, *2*, *3*, *4*) are the results of calculations for the TM_{01} mode in the waveguide with ideally conducting walls at $\varepsilon = 1$ (hollow waveguide), 1.5^2 (SiO_2), 2.4^2 (Si_3N_4), 3.5^2 (Si), respectively.

performed for the aluminium-coated waveguide and fused silica core at $\lambda = 488$ nm.

(ii) The comparison of the results of this paper with those obtained for the case of the ideal metal allow the conclusion to be drawn that the behaviour of the complex reflection coefficient as a function of ka is qualitatively the same in both cases under the condition the evanescent mode under study exists in the waveguide ($0.3967 < ka < 1.4364$). At $ka < 0.39667$, the mode under study disappears in the aluminium-coated waveguide, which means that the ideal-metal model is inapplicable in this region. The differences in the results for the waveguides with the real metal and ideal metal walls increase with ka and become the largest in the vicinity of the point $ka = 1.4364$, starting from which the evanescent mode is transformed into the propagating one.

(iii) Calculations of the far-field transmission coefficient of the nanowaveguide show that it strongly depends on the dielectric constant of the waveguide core and the type of waveguide modes. In particular, the transmission coefficient for transverse-magnetic mode TM_{01} is an order of magnitude higher than that for the transverse-electric mode TE_{01}. Both coefficients markedly differ from the value yielded by the classical Bethe theory in the case of the transmission of a plane linearly-polarised wave through the subwavelength aperture in an ideally conducting screen.

(iv) We can conclude from our calculations for the aluminium that despite a substantial influence of optical constants for the real metal on the behaviour of the fields inside and outside the waveguide, the model of an ideal metal has a rather broad range of applications if the dielectric constant of the waveguide walls is large enough in modulus. However, one should expect that the influence of resonance plasmon effects during the transmission of light through the waveguide nanoaperture will be especially strong for waveguides with walls made of noble metals (similar to that as it is in the case of nanoholes in the silver and gold films).

Acknowledgements. This work was supported by the Russian Foundation for Basic Research (Grant Nos 09-02-01024 and 07-02-00873), the 'Development of the Scientific Potential of the Higher School' program (Project No. 2.1.1/4294) and by programs 'Optical Spectroscopy and Frequency Standards' and 'Coherent Optical radiation of Semiconductor Compounds and Structures' of the Department of Physical Sciences, RAS.

References

1. Kuznetsova T.I., Lebedev V.S. *Kvantovaya Elektron.*, **39**, 455 (2009) [*Quantum Electron.*, **39**, 455 (2009)].
2. Thio T., Pellerin K.M., Linke R.A., Lezec H.J., Ebbesen T.W. *Opt. Lett.*, **26**, 1972 (2001).
3. Lezec H.J., Degiron A., Devaux E., Linke R.A., Martin-Moreno L., Garcia-Vidal F.J., Ebbesen T.W. *Science*, **297**, 820 (2002).
4. Ebbesen T.W., Lezec H.J., Ghaemi H.F., Thio T., Wollf P.A. *Nature (London)*, **391**, 667 (1998).
5. Bonod N., Enoch S., Li L., Popov E., Nevière M. *Opt. Express*, **11**, 482 (2003).
6. Degion A., Lezec H.J., Yaamoto N., Ebbesen T.W. *Opt. Commun.*, **239**, 61 (2004).
7. Yin L., Vlasko-Vlasov V.K., Rydh A., Pearson J., Welp U., Chang S.-H., Gray S.K., Schatz G.C., Brown D.B., Kimball C.W. *Appl. Phys. Lett.*, **85**, 467 (2004).
8. Chang S.-H., Gray S.K., Schatz G.C. *Opt. Express*, **13**, 3150 (2005).
9. Rindzevicius T., Alaverdyan Y., Sepulveda B., Pakizeh T., Kall M., Hillenbrand R., Aizpurua J., Garcia de Abajo F.J. *J. Phys. Chem. C*, **111**, 1207 (2007).
10. Shuford K.L., Gray S.K., Ratner M.A., Schatz G.C. *Chem. Phys. Lett.*, **435**, 123 (2007).
11. Garcia-Vidal F.J., Martin-Moreno L. *Phys. Rev. B*, **66**, 155412 (2002).
12. Martin-Moreno L., Garcia-Vidal F.J., Lezec H.J., Degiron A., Ebbesen T.W. *Phys. Rev. Lett.*, **90**, 167401 (2003).
13. Degiron A., Ebbesen T.W. *Opt. Express*, **12**, 3694 (2004).
14. Ghaemi H.F., Thio T., Grupp D.E., Ebbesen T.W., Lezec H.J. *Phys. Rev. B*, **58**, 6779 (1998).
15. Popov E., Nevière M., Enoch S., Reinisch R. *Phys. Rev. B*, **62**, 16100 (2000).
16. Martin-Moreno L., Garcia-Vidal F.J., Lezec H.J., Pelerin K.M., Thio T., Pendry J.B., Ebbesen T.W. *Phys. Rev. Lett.*, **86**, 1114 (2001).
17. Wannemacher R. *Opt. Commun.*, **195**, 107 (2001).
18. Sarrazin M., Vigneron J.-P., Vigoureux J.-M. *Phys. Rev. B*, **67**, 085415 (2003).
19. Keilmann F. *J. Microsc.*, **194**, 567 (1999).
20. Yatsui T., Isumi K., Kourogi M., Ohtsu M. *Appl. Phys. Lett.*, **80**, 2257 (2002).
21. Bouhelier A., Renger J., Beversluis M.R., Novotny L. *J. Microsc.*, **210**, 220 (2003).
22. Novotny L., Hafner C. *Phys. Rev. E*, **50**, 4094 (1994).
23. Prade B., Vinet J.Y. *J. Lightwave Technol.*, **12**, 6 (1994).
24. Bethe H.A. *Phys. Rev.*, **66**, 163 (1944).
25. Bouwkamp C.J. *Rep. Prog. Phys.*, **17**, 35 (1954).